Int. J. Heat Mass Transfer. Vol. 36, No. 11, pp. 2759–2768, 1993
Printed in Great Britain

0017–9310/93 $6.00+0.00

A two-phase mixture model of liquid–gas flow and heat transfer in capillary porous media—II. Application to pressure-driven boiling flow adjacent to a vertical heated plate

CHAO-YANG WANG and C. BECKERMANN
Department of Mechanical Engineering, The University of Iowa, Iowa City, IA 52242, U.S.A.

(*Received* 16 *December* 1991 *and in final form* 7 *December* 1992)

Abstract—The two-phase mixture model developed in Part I is applied to investigate a pressure-driven two-phase boiling flow along a heated surface embedded in a porous medium. The general governing equations in Part I for the transport of mass, momentum and liquid (constituent) mass for the two-phase mixture are simplified for the above system. The present formulation, owing to its strong analogy to the classical description of multicomponent convective flows, suggests that a thin capillary layer exists over the solid surface at high Peclet numbers and that the two-phase flow is confined only to this boundary layer. Using approximations analogous to the classical boundary layer theory, a set of boundary layer equations for two-phase flow is derived and solved by a similarity transformation. The resulting ordinary differential equations are numerically integrated using a combination of the Gear stiff method and a shooting procedure. Numerical results for the saturation field and the flow fields of the two-phase mixture and the individual phases are presented and discussed.

1. INTRODUCTION

IN ORDER to demonstrate the utility of the two-phase mixture model developed in our previous paper [1], referred to as Part I hereafter, we analyze a practical problem of both academic and engineering interest, that is, two-phase boiling flow along a heated body embedded in a porous medium. This problem has become increasingly important in many engineering applications, including, for example, the cooling of an igneous intrusion in a geothermal reservoir [2], the *in situ* removal of thermal energy from nuclear reactor debris formed by a degraded core accident [3], the geological repository of high-level nuclear waste packages [4, 5], and the transport processes inside heat pipes [6].

A survey of the literature reveals that a great number of analytical studies on boiling in a porous medium adjacent to a heated surface have appeared during the past decade. For example, in the pioneering works of Parmentier [7] and Cheng and Verma [8] the boiling process in the neighborhood of a vertical heated plate in a porous medium filled with a quiescent liquid was modeled. Later, Orozco *et al.* [9] extended the analysis to cylindrical and spherical geometries. Other hydrodynamic and thermal aspects of the problem, such as the effects of liquid subcooling, main flow, tilting angles of plates, and the inclusion of non-Darcian terms, have also been thoroughly addressed in the subsequent literature. However, all these investigations have assumed a negligible capillary force resulting from liquid–vapor interfacial tension. As a result, it has been presumed that the vapor and liquid phases are completely separate. That is, two single-phase layers separated by a distinct interface are formed adjacent to the heated surface. Thus, the problem is greatly simplified and can be formulated using single-phase governing equations. Analytical solutions have been obtained at the expense of neglecting the two-phase characteristics that are inherent in this class of problems.

Recently, however, experimental evidence [10–12] has strongly suggested that the inclusion of capillary effects in a theoretical model is necessary to achieve quantitative agreement with experimental data. Thus, an analysis is required for the transport phenomena inside the two-phase mixed zone that appears when the capillary effect is included.

A boiling flow along a heated surface immersed in a porous medium is analyzed in this study. Specifically, the special case is considered where a pure liquid at its boiling temperature is forced to pass along a hot surface where it is partially boiled into vapor. The present investigation is limited to pressure-driven two-phase flow, while buoyancy effects are not taken into account. Furthermore, a constant liquid saturation is assumed to be present at the surface. It is shown that, via the formulation developed in Part I, a semi-analytical solution is possible. Moreover, a similarity solution exists for the present problem within the classical boundary layer approximation well known in single-phase fluid dynamics, thereby addressing a

NOMENCLATURE

a_0	constant in equation (43)
D	capillary diffusion coefficient, equation (4)
D_c	constant part of capillary diffusion coefficient, equation (7)
$\hat{D}$	dimensionless capillary diffusion coefficient, equation (8)
F	stream function, equation (31)
h_{fg}	latent heat of phase change
J	capillary pressure function
$\mathbf{j}$	diffusive mass flux
K	absolute permeability
k_r	relative permeability
L	plate length
p	pressure
P	scaled pressure
$Pe_{2\phi}$	two-phase Peclet number, equation (16)
q	heat flux
Q_w	dimensionless local wall heat flux, equation (21)
s	liquid saturation
$\mathbf{u}$	velocity vector
u	velocity in x-direction
U	scaled velocity in x-direction
v	velocity in y-direction
V	scaled velocity in y-direction
x	coordinate normal to the plate
X	transformed x-coordinate
y	coordinate along the plate
Y	transformed y-coordinate.

Greek symbols

β	dimensionless viscosity function
γ	dimensionless density function
$\Delta\rho$	$\rho_l - \rho_v$
δ	boundary layer thickness
ε	small value, equation (23)
η	similarity variable
λ	relative mobility
μ	viscosity
ν	kinematic viscosity
ρ	density.

Subscripts

dry	dryout state
i	irreducible
l	liquid
max	maximum
v	vapor
w	wall
δ	two-phase boundary layer
∞	infinite.

Superscripts

	ratio of properties of liquid to vapor
—	average
*	dimensionless
′	derivative with respect to η.

novel aspect of boiling flows over heated surfaces in porous media that, to date, appears to have been unnoticed. The general formulation of the problem is given in Section 2, while in Section 3 the boundary layer approximations are invoked. The similarity transformation is developed in Section 4. Numerical procedures are detailed in Section 5, and the results of the calculations are reported and discussed in Section 6. The results include the liquid saturation distribution as well as the flow fields of the two-phase mixture and the individual phases.

2. FORMULATION

We consider a heated flat plate which is submerged in an infinite porous medium, as depicted in Fig. 1. The porous structure is filled with a liquid passing, with a constant velocity, u_∞, over the surface under an external pressure difference. The heat input over the surface is sufficiently high to induce evaporation and/or boiling in its vicinity. As a consequence, a two-phase region, consisting simultaneously of liquid and vapor, is formed adjacent to the solid surface. The two-phase flow in this mixed zone is the object of the present investigation.

The liquid saturation, a conventional concept in the field of multi-phase flow through porous media, equals unity at a location far from the surface, while it is assumed to be uniform at the surface. A dryout condition is reached when the liquid saturation at the surface approaches zero, which implies that the liquid evaporates completely in the immediate neighborhood of the plate. This critical condition is characterized by a certain value of the heat flux, which is similar to the critical heat flux in pool boiling in an open space. As the heat flux increases further, a pure vapor film forms over the heated plate and continues to grow, finally leading to a meltdown of the plate material. Although the present analysis is restricted to the regime prior to dryout, it is, nevertheless, possible to deal with the post-dryout regime by combining the present results with traditional film flow analyses such as those given in refs. [13, 14].

As in Part I, we treat the two-phase mixture essentially as a binary mixture whose transport properties depend only on the local concentration (liquid satu-

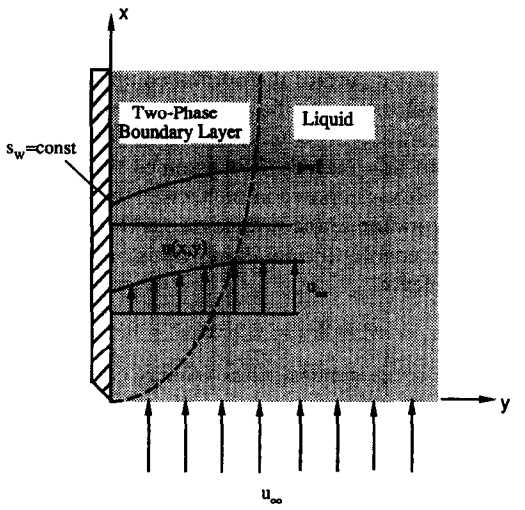

FIG. 1. Schematic diagram of pressure-driven boiling two-phase flow in porous media.

ration), s. The mean density and kinematic viscosity, as obtained in Part I, are:

$$\rho(s) = \rho_l \gamma(s) \equiv \rho_l \left[1 - \frac{\Delta\rho}{\rho_l}(1-s)\right] \tag{1}$$

and

$$v(s) = v_l \beta(s) \equiv v_l \left[k_{rl}(s) + \frac{v_l}{v_v} k_{rv}(s)\right]^{-1} \tag{2}$$

where ρ_l and v_l are the density and viscosity of the liquid, respectively, and $\Delta\rho = \rho_l - \rho_v$ with ρ_v being the density of the vapor. Likewise, v_v is the kinematic viscosity of the vapor. The terms $\gamma(s)$ and $\beta(s)$ denote the coefficients of the mean density and viscosity, respectively, and $k_{rl}(s)$ and $k_{rv}(s)$ are the relative permeabilities of the two phases. In addition, we utilize the concept of a total diffusive mass flux, $\mathbf{j}$, of a constituent (phase), which is a combination of the capillary diffusive flux and the gravity-induced migrating flux [1]. Since the latter flux is assumed to be negligible in the present study, the total diffusive mass flux simply reduces to

$$\mathbf{j} = -D(s)\nabla s \tag{3}$$

where the capillary diffusion coefficient, $D(s)$, is linearly proportional to the gradient of the capillary pressure, which in turn, is a function of the local liquid saturation, s. Assuming that, to a first approximation, this diffusivity is isotropic, we express the capillary diffusion coefficients as [1]

$$D(s) = \frac{K}{v(s)}\lambda(s)[1-\lambda(s)]\left[-\frac{\mathrm{d}p(s)}{\mathrm{d}s}\right] \equiv D_c \hat{D} \tag{4}$$

where $\lambda(s)$ is the relative mobility given by [1]

$$\lambda = \frac{k_{rl}(s)}{k_{rl}(s) + \bar{v}k_{rv}(s)} \tag{5}$$

with $\bar{v}$ denoting the ratio of the liquid and vapor kinematic viscosities; i.e.

$$\bar{v} = v_l / v_v. \tag{6}$$

The term D_c in equation (4) is the constant part of the saturation-dependent capillary diffusion coefficient; i.e.

$$D_c = (\varepsilon K)^{1/2}\sigma / v_l \tag{7}$$

and $\hat{D}$ denotes the dimensionless capillary diffusion coefficient encompassing all variable factors

$$\hat{D}(s) = \frac{\lambda(s)[1-\lambda(s)]}{\beta(s)}\left[-\frac{\mathrm{d}J(s)}{\mathrm{d}s}\right] \tag{8}$$

with $J(s)$ being the capillary function, which is assumed to depend on the liquid saturation only. The basic transport functions $k_{rl}(s)$, $k_{rv}(s)$ and $J(s)$ are taken to be known, and their explicit forms used in this analysis are provided in Section 5.

2.1. *Basic equations*

The general equations governing the transport of mass, momentum and energy for two-phase mixtures in porous media were derived in Part I. These are simplified for the present problem by assuming that the boiling flow is: (1) steady; (2) isothermal across the entire two-phase region; (3) driven purely by an external pressure difference so that the pure liquid outside the two-phase region has a uniform upward velocity and gravitational effects are absent; and (4) heated solely by the surface. Then we have:

conservation of mixture mass:

$$\nabla\cdot(\rho\mathbf{u}) = 0 \tag{9}$$

conservation of mixture momentum:

$$\mathbf{u} = -\frac{K}{\rho(s)v(s)}\nabla p \tag{10}$$

conservation of liquid mass:

$$\nabla\cdot[\rho\mathbf{u}\lambda(s)] = -\nabla\cdot\mathbf{j}. \tag{11}$$

With the continuity equation and the definition of $\mathbf{j}$ given in equation (3), the conservation equation for liquid mass can be rewritten as

$$\frac{\mathrm{d}\lambda}{\mathrm{d}s}\rho\mathbf{u}\cdot\nabla s = D_c\nabla\cdot(\hat{D}\nabla s). \tag{12}$$

In the above equations, $\mathbf{u}$ and p denote the velocity vector and pseudo pressure, respectively, of a flowing mixture consisting of liquid and vapor phases, as defined in Part I.

Scalar equations (9) and (12) and vectorial equation (10) constitute a full system for four unknowns: the pressure, liquid saturation and two velocity components. To simplify further, equations (9), (10) and (12) are rendered dimensionless using L and u_∞ as the characteristic length and velocity, respectively. Thus the governing equations become

$$\nabla \cdot (\gamma(s)\mathbf{u}^*) = 0 \tag{13}$$

$$\mathbf{u}^* = -\frac{1}{\gamma(s)\beta(s)}\nabla p^* \tag{14}$$

$$\frac{\mathrm{d}\lambda}{\mathrm{d}s}\gamma(s)\mathbf{u}^* \cdot \nabla s = \frac{1}{Pe_{2\phi}}\nabla \cdot (\hat{D}\nabla s) \tag{15}$$

where the superscript * denotes dimensionless variables. The two-phase Peclet number in equation (15) is defined as

$$Pe_{2\phi} = \frac{\rho_l u_\infty L}{D_c} \tag{16}$$

which is based on the capillary diffusion coefficient. Though primarily introduced for the sake of simplicity, the two-phase Peclet number does have a physical interpretation similar to that of its counterpart in the single-phase case. In addition, it should be noted that in its definition we have employed the constant part, D_c, of the capillary diffusion coefficient, but not its real magnitude, $D_c\hat{D}_{max}$. This is because $\hat{D}_{max}$ varies widely depending on the constitutive relations chosen (see below). Not using $D_c\hat{D}_{max}$, thus, makes the formulation more general and convenient. In adopting such a formulation, however, it should be kept in mind that $\hat{D}_{max}$ may be several orders of magnitude smaller than unity.

It is clear from equation (15) that the influence of capillary diffusion depends on the value of $\hat{D}_{max}/Pe_{2\phi}$, or in another form, $\rho_l u_\infty L/D_c\hat{D}_{max}$. This value can be much larger than unity for low-permeability porous media. Based on the relative permeabilities and the capillary pressure function given in Section 5, Table 1 gives typical values of $D_c\hat{D}_{max}$ for a porous matrix with the porosity assumed to be 0.5 and for various fluids. It can be seen that the magnitude of $D_c\hat{D}_{max}$ is comparable to that of the liquid dynamic viscosity.

2.2. *Boundary conditions*

At the leading edge of the plate and outside the two-phase region, the liquid saturation is unity. In addition, for a constant external pressure difference, equation (10) indicates that the bulk liquid flows with a constant velocity. Hence, the following conditions apply

$$u^* = 1, s = 1 \quad \text{at } x^* = 0,$$
$$\text{and for } y^* \gg \delta^* \text{ when } x^* > 0 \tag{17}$$

where u^* denotes the dimensionless velocity component in the x-direction and δ^* the dimensionless thickness of the two-phase region.

On the solid surface the normal component of the mixture velocity must be equal to zero. Either the liquid saturation or its gradient also needs to be prescribed. In this analysis, it is assumed that the local wall heat flux is imposed in such a way that a uniform liquid saturation at the surface results (this boundary condition enables the similarity transformation; see below). Hence

$$v^* = 0, s = s_w \quad \text{at } y^* = 0 \tag{18}$$

where v^* is the dimensionless velocity component in the y-direction. For $s_w = 0$, dryout occurs at the wall. Once s_w is specified, the wall heat flux distribution, $q_w(x)$, must be obtained as part of the solution; it is determined by the energy balance at the wall, i.e.

$$q_w = h_{fg} \cdot (-j_w) \tag{19}$$

where j_w is the total diffusive mass flux at the wall and is given by

$$j_w = -D_c\hat{D}\left.\frac{\partial s}{\partial y}\right|_{y=0}. \tag{20}$$

Combining equations (19) and (20) and introducing a dimensionless wall heat flux,

$$Q_x = \frac{q_w x}{h_{fg} D_c} \tag{21}$$

we have

$$Q_x = -\hat{D}x^*\left.\frac{\partial s}{\partial y^*}\right|_{y^*=0}. \tag{22}$$

3. BOUNDARY LAYER APPROXIMATIONS

Now we consider two-phase flow over a flat plate within the two-dimensional geometry depicted in Fig. 1. Because the governing equations (13)–(15) and boundary conditions (17) and (18) strongly resemble the mathematical description of a convective mass transfer process in porous media, it is desirable to simplify equations (14) and (15) by invoking the classical boundary layer approximations, as in single-phase fluid dynamics. This approximation is valid if the two-phase Peclet number is much larger than unity. To this end, a perturbation scheme is first established in which

Table 1. Typical values of the capillary diffusion coefficient ($D_c\hat{D}_{max}$) for various fluids and porous media [kg m s^{-1}]

Fluids	Viscosity μ_l [kg m s^{-1}]	Permeability, K [m^2]			
		10^{-8}	10^{-10}	10^{-11}	10^{-12}
Water	2.85×10^{-4}	2.46×10^{-2}	2.46×10^{-3}	7.78×10^{-4}	2.46×10^{-4}
Freon-113	4.94×10^{-4}	6.14×10^{-3}	6.14×10^{-4}	1.94×10^{-4}	6.14×10^{-5}
Ethanol	4.28×10^{-4}	3.86×10^{-3}	3.86×10^{-4}	1.22×10^{-4}	3.86×10^{-5}

$$\varepsilon = \frac{1}{\sqrt{Pe_{2\phi}}} \equiv \frac{1}{\sqrt{(\rho_l u_\infty L/D_c)}} \ll 1 \tag{23}$$

is chosen as the perturbation parameter. Then the appropriate scaling transformation is

$$Y = y^*/\varepsilon, \quad X = x^*, \quad U = u^*, \quad V = v^*/\varepsilon, \quad P = p^*. \tag{24}$$

In light of the smallness of ε, these transformations imply that the velocity component along the vertical surface dominates the one perpendicular to it, and that changes across the boundary layer are much steeper than those along it.

Substituting the above transformations into the system of equations (13)–(15) and ordering according to powers of ε, the following is obtained:

$$\frac{\partial(\gamma(s)U)}{\partial X} + \frac{\partial(\gamma(s)V)}{\partial Y} = 0 \tag{25}$$

$$U = -\frac{1}{\gamma(s)\beta(s)}\frac{\partial P}{\partial X} \tag{26}$$

$$-\frac{\partial P}{\partial Y} = O(\varepsilon^2) \tag{27}$$

$$\frac{d\lambda}{ds}\gamma(s)\left(U\frac{\partial s}{\partial X} + V\frac{\partial s}{\partial Y}\right) = \frac{\partial}{\partial Y}\left(\hat{D}\frac{\partial s}{\partial Y}\right) + O(\varepsilon^2). \tag{28}$$

The corresponding boundary conditions at $Y = 0$ and $Y \to \infty$ become

$$Y = 0; \quad V = 0 \quad \text{and} \quad s = s_w \tag{29}$$

$$Y \to \infty; \quad U = 1 \quad \text{and} \quad s = 1. \tag{30}$$

Equations (25)–(28) imply that the present two-phase flow and the changes in the liquid saturation occur only within a thin boundary layer in the vicinity of the surface. Thus, if a steady-state is to prevail, the vapor generated at the wall must be carried downstream by the flow parallel to the surface.

There is an obvious similarity between equations (25)–(28) and the corresponding boundary layer equations for porous media convective mass transfer adjacent to a surface. However, a fundamental difference that appears in the mean transport properties should be noted. The mean properties of the two-phase mixture exhibit drastic variations with liquid saturation (see below), so that it is impossible to make the constant-property assumption as is usually done in the classical treatment of single-phase boundary layer flows. A more elaborate procedure is called for to deal with the difficulty arising from variable properties.

4. A SIMILARITY TRANSFORMATION

As shown above, when $\varepsilon \ll 1$, a system of boundary layer equations can be obtained. Hence, the existence of a similarity solution can be anticipated and, indeed, it is easy to show that the appropriate transformation is

$$\gamma(s)U = F'(\eta), \quad s = s(\eta) \tag{31}$$

where

$$\eta = Y/X^{1/2} \tag{32}$$

with the prime denoting differentiation with respect to η. The use of the continuity equation yields

$$\gamma(s)V = (\tfrac{1}{2}\eta F' - \tfrac{1}{2}F)X^{-1/2} \tag{33}$$

where F is the dimensionless stream function. Eliminating the pressure P between equations (26) and (27) by cross differentiating and then substituting equation (33) into the resulting equation, as well as into equation (28), yields

$$(\beta(s)F')' = 0 \tag{34}$$

and

$$(\hat{D}s')' + \frac{1}{2}\frac{d\lambda(s)}{ds}Fs' = 0. \tag{35}$$

The boundary conditions are transformed correspondingly into

$$F = 0 \quad \text{and} \quad s = s_w \quad \text{at} \quad \eta = 0 \tag{36}$$

and

$$F' = 1 \quad \text{and} \quad s = 1 \quad \text{at} \quad \eta = \eta_\delta \tag{37}$$

with $\eta = \eta_\delta$ denoting the outer edge of the capillary layer where the longitudinal velocity component and liquid saturation match those at infinity.

It is interesting to note that when all mean properties of the two-phase mixture are constant, the above similarity equations reduce to the familiar version for forced convective mass transfer in porous media.

5. SOLUTION PROCEDURES

In order to solve the similarity equations, equations (34) and (35) subject to equations (36) and (37), functional forms of $k_{rl}(s)$, $k_{rv}(s)$ and $J(s)$ must be explicitly specified. Following Fatt and Klikoff [15], we assume that the relative permeabilities can be expressed as

$$k_{rl} = S^3, \quad k_{rv} = (1-S)^3 \tag{38}$$

where k_{rl} and k_{rv} are functions of the normalized liquid saturation, defined as:

$$S = \frac{s - s_{li}}{1 - s_{li}} \tag{39}$$

where s_{li} is the irreducible liquid saturation. For the sake of simplicity, s_{li} is set to zero; therefore $S = s$. The capillary pressure function $J(s)$ is assumed to be of the form [16]

$$J(s) = 1.417(1-S) - 2.120(1-S)^2 + 1.263(1-S)^3 \tag{40}$$

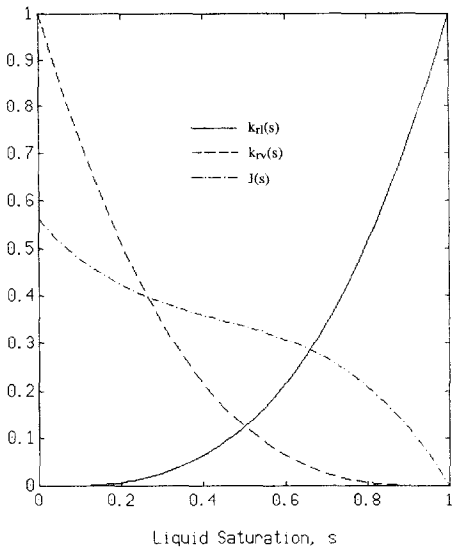

FIG. 2. Constitutive relationships as functions of the normalized liquid saturation.

which is an empirical correlation fitted to Leverett's experimental data [17].

Figure 2 schematically shows the above constitutive relationships, while Fig. 3 displays the corresponding mean properties for a water–steam mixture. All quantities are normalized by their corresponding maximum values in order to show them in a single graph. While other physically reasonable functional forms of the constitutive relationships can be chosen, this is expected to only affect the quantitative features of the results presented below.

Equations (34) and (35) are numerically solved

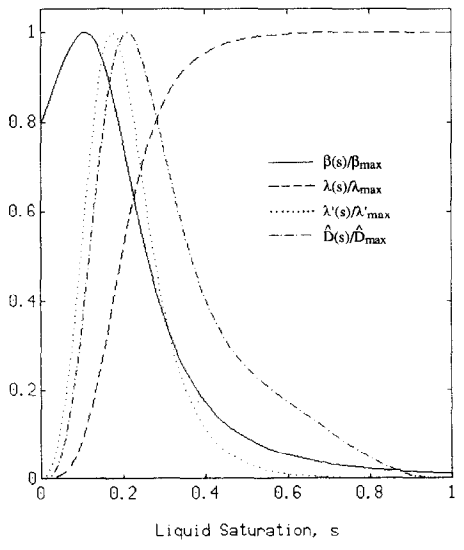

FIG. 3. Normalized mean properties of the water–steam mixture with respect to the normalized liquid saturation, obtained by using the constitutive relationships shown in Fig. 2 and with $\beta_{max} = 85.71$; $\lambda'_{max} = 4.959$ and $\hat{D}_{max} = 1.7541 \times 10^{3}$.

using the IMSL [18] subroutine DGEAR which is based on the Gear stiff method. The use of this stiff method is needed, because the liquid saturation grows exponentially very near the wall, but rather slowly at a small distance away from it. Therefore, a variable step size was employed which can be made as small as is needed for a desired accuracy and stability, but increased whenever possible to reduce the total computer time needed. As an indicator of the stiffness of the differential equations, the IMSL subroutine DVERK, which uses the standard fourth-order Runge–Kutta method, was also used at the initial stage of this numerical work. However, as s_w was reduced below 0.15, this attempt was fruitless.

In addition, a shooting procedure is incorporated which initiates the integration by guessing the value of $s'(0)$ and adjusting this guess until the saturation becomes unity outside the boundary layer. To satisfy the boundary conditions at the edge of the two-phase layer, the integration length must be chosen to be greater than the boundary layer thickness. Although this thickness depends on the wall liquid saturation, as shown in Table 2, a distance of $\eta = 2$ was found to be adequate in all numerical runs.

Another difficulty associated with the present numerical implementation is the singularity of the problem at $\eta = 0$, when the wall saturation approaches zero (i.e. the dryout condition), since the capillary diffusion coefficient drops to zero in this case. In order to overcome this difficulty, we develop an analytical solution of equations (34) and (35), which is valid only near the phase-change surface. To this end, equation (34) is first integrated once and boundary condition (37) is applied to give

$$\beta(s)F' = 1. \tag{41}$$

For $s \to 0$, equations (41) and (35) reduce to

$$\left.\begin{aligned} F' &= \bar{v} \\ [-J'(0)]\frac{\mathrm{d}}{\mathrm{d}\eta}\left(s^3\frac{\mathrm{d}s}{\mathrm{d}\eta}\right) + \frac{3}{2\bar{v}}Fs^2\frac{\mathrm{d}s}{\mathrm{d}\eta} &= 0 \end{aligned}\right\} \quad \eta \ll 1. \tag{42}$$

By seeking a series expansion solution, we find

$$\left.\begin{aligned} F &= \bar{v}\eta \\ s &= a_0\eta^{1/4} - \frac{24}{77[-J'(0)]}\eta^2 + \cdots \end{aligned}\right\} \quad \eta \ll 1, \tag{43}$$

Table 2. Summary of numerical solutions

s_w	η_δ	$s'(0)$	$Q_x/(Pe_{2\phi}X)^{1/2}$
0.0	1.689	0.2782†	1.451×10^{-3}
0.2	1.625	0.6354	1.107×10^{-3}
0.4	1.388	0.5526	3.952×10^{-4}
0.6	1.170	0.3892	1.181×10^{-4}
0.8	0.850	0.1697	1.434×10^{-5}

† It is the value of a_0 in this singular case.

where a_0 is a constant to be determined. This approximate solution is then used to give the starting values for the numerical solution of equations (34) and (35) for the stream function and saturation profiles across the entire boundary layer. In this singular case, the shooting aim is replaced to find the constant a_0 rather than to determine the saturation gradient $s'(0)$.

6. RESULTS AND DISCUSSION

Examination of the similarity equations reveals that the solution solely depends on the viscosity ratio, $\bar{v}$, of a system. For the purpose of providing an illustrative example, calculations are performed for a water–steam system at atmospheric pressure. Thus, the value of $\bar{v}$ is fixed at 0.01466. Although the density ratio also has a substantial influence on the physical behavior of the system considered, it does not enter the present solution because the stream function defined in equation (31) incorporates the density effect and the numerical results for the velocity fields are properly scaled (see below).

6.1. *Results for two-phase mixture properties*

Results are first presented for the two-phase mixture properties, namely the liquid saturation, $s(\eta)$, the scaled axial mixture velocity, $\gamma u^*(\eta)$, and the scaled transverse mixture velocity, $\gamma v^*(\eta)(X\,Pe_{2\phi})^{1/2}$. These are shown in Figs. 4–6 as functions of the wall saturation, s_w.

The saturation profiles in Fig. 4 show several peculiar features. First, their overall shapes are complex in that their curvature change signs at various stages (most obviously from the curve corresponding to $s_w = 0$). This is in contrast to the simple curve with a uniquely negative curvature found in convective mass transfer problems. The difference can be attributed to the fact that the mean transport properties of the two-phase mixture are highly nonlinear and even exhibit maxima at certain saturations, as can be seen from Fig. 3. Second, because the capillary diffusion coefficient becomes small as the liquid saturation approaches unity, the saturation profiles show boundary layers with relatively sharp edges. Last, as anticipated, the two-phase boundary layer expands as the wall saturation decreases. The present numerical solution can also provide quantitative information on the boundary layer thickness δ, i.e. the size of the two-phase zone. In this regard, we suppose that the edge of the boundary layer, i.e. at $y^* = \delta^*$, is the point where s has a value of 0.99, and let η_δ denote the value of η at this point. It follows from equation (32) that

$$\delta^* = \eta_\delta (x^*/Pe_{2\phi})^{1/2}. \tag{44}$$

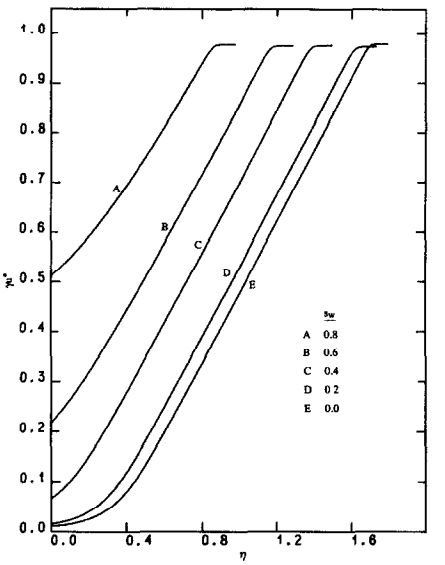

FIG. 5. Scaled axial mixture velocity profiles γu^* in the two-phase boundary layer for several values of the wall saturation.

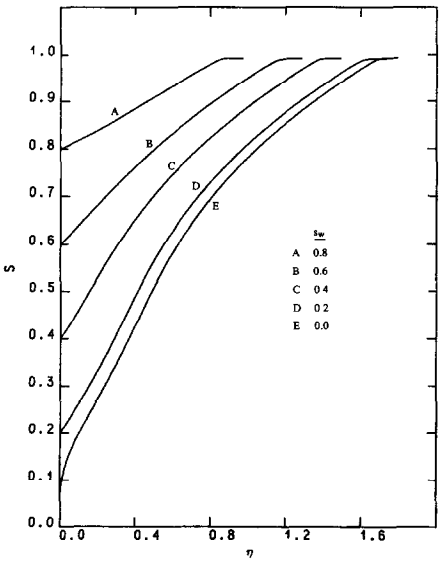

FIG. 4. Liquid saturation profiles vs η for several values of the wall saturation.

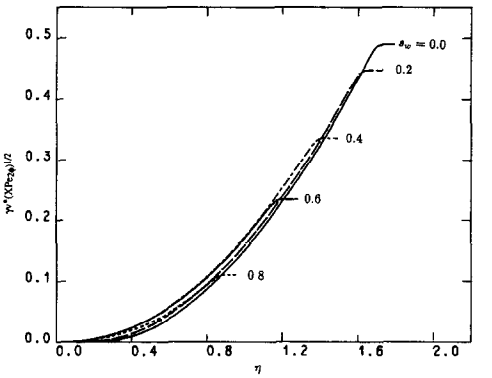

FIG. 6. Scaled transverse mixture velocity profiles $\gamma v^*(X\,Pe_{2\phi})^{1/2}$ in the two-phase boundary layer for several values of the wall saturation.

The values of η_δ for different wall saturations are tabulated in Table 2.

The scaled axial velocity profiles γu^* shown in Fig. 5 also show a novel aspect: the velocity gradually decreases toward the wall, just as the liquid saturation does. Presumably this is due to the variable kinematic viscosity of the two-phase mixture. Because the vapor kinematic viscosity is much larger than that of the liquid, the mean viscosity of the mixture increases as the liquid composition decreases toward the wall, and therefore the mixture motion is retarded there. In the limiting case where the wall saturation approaches zero, the mixture in the immediate neighborhood of the wall becomes almost motionless axially. It should be cautioned that this apparent no-slip condition does not result from the so-called Brinkman modification of Darcy's law, but from the strong interrelation between the flow and liquid saturation fields. It is because of this high degree of coupling that a two-phase problem like that considered here is not amenable to analytical solutions.

The positive values of the scaled transverse velocity profiles $\gamma v^*(X\,Pe_{2\phi})^{1/2}$ shown in Fig. 6 indicate that there is a displacement flow toward the outside of the boundary layer. Furthermore, more fluid is displaced as the wall saturation decreases. This behavior results from the fact that liquid flowing inside the boundary layer evaporates into vapor, forming a two-phase mixture that slows down due to the higher viscosity of the two-phase boundary layer, and is thus forced outside the layer because of continuity requirements. The viscous displacement is similar to that observed in boundary layer flows of single-phase fluids.

6.2. *Flow fields of the individual phases*

As stated in Part I, the present mixture model is capable not only of providing information on the flow field of the two-phase mixture as a whole, but also of predicting the flow fields of the individual phases. This is realized through the following relationships, established in Part I:

$$\rho_l \mathbf{u}_l = \mathbf{j} + \lambda \rho \mathbf{u} \tag{45}$$

and

$$\rho_v \mathbf{u}_v = -\mathbf{j} + (1-\lambda)\rho \mathbf{u}. \tag{46}$$

Rendered dimensionless by using u_∞ as the characteristic velocity, these relationships can be rewritten in explicit component form as

$$\begin{cases} u_l^* = \lambda(s)F'(\eta) + \varepsilon^2[\hat{D}(s)s'(\eta)\eta/2X] \\ v_l^* = \varepsilon X^{-1/2}\left[\dfrac{\lambda}{2}(\eta F' - F) - \hat{D}(s)s'(\eta)\right] \end{cases} \tag{47}$$

and

$$\begin{cases} \bar{\rho} u_v^* = (1-\lambda)F'(\eta) - \varepsilon^2[\hat{D}(s)s'(\eta)\eta/2X] \\ \bar{\rho} v_v^* = \varepsilon X^{-1/2}\left[\dfrac{1-\lambda}{2}(\eta F' - F) + \hat{D}(s)s'(\eta)\right] \end{cases} \tag{48}$$

with $\bar{\rho}$ denoting ρ_v/ρ_l.

Figures 7(a) and (b) depict the vapor flow field $\bar{\rho}\mathbf{u}_v^*$ and liquid flow field $\mathbf{u}_l^*$, respectively, in a two-phase boundary layer corresponding to zero wall saturation. The dotted line in these plots represents the edge of the boundary layer. A co-current upward two-phase flow is predicted as a result of the direction of the applied external pressure difference. The vapor moves primarily vertically except in the near-wall region where it is laterally generated. With increasing distance from the wall, both components of the velocity diminish to zero, indicating that all vapor produced at the wall is carried downstream. Outside the boundary layer, the void space is occupied by liquid.

Conversely, near the wall, the liquid velocity gradually vanishes because the liquid continuously becomes

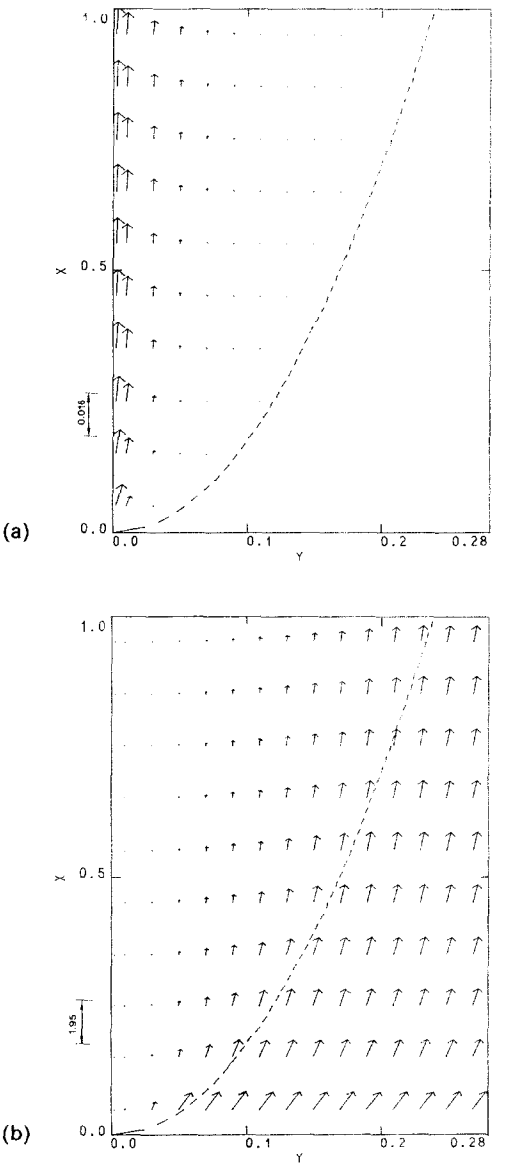

FIG. 7. Plots of flow fields for both phases: (a) vapor velocity $\bar{\rho}\mathbf{u}_v^*$; (b) liquid velocity $\mathbf{u}_l^*$. The dotted line denotes the two-phase boundary layer edge.

vapor. In addition, the liquid has considerable lateral motion both inside and outside the boundary layer, owing to the viscous displacement effect mentioned earlier.

6.3. *Wall heat flux*

It is of interest to determine the distribution of the wall heat flux which corresponds to the constant liquid saturation condition imposed at the wall. Rewriting equation (22) in terms of the similarity variables yields

$$Q_x/\sqrt{(Pe_{2\phi}\,X)} = \hat{D}(s_w)[s'(0)] \quad s_w \neq 0. \tag{49}$$

In the singular case ($s_w = 0$), equation (49) should be modified as

$$Q_x/\sqrt{(Pe_{2\phi}\,X)} = 0.2415a_0^4 \quad s_w = 0. \tag{50}$$

As anticipated, Q_x is proportional to the square root of both the Peclet number and the dimensionless axial length. The proportionality coefficients are given in Table 2 and also shown in Fig. 8. It can be observed that $Q_x/\sqrt{(Pe_{2\phi}\,X)}$ increases as the wall saturation is reduced, finally converging to a constant value equaling 1.451×10^{-3}, which is the dryout limit.

An integration procedure yields the following average heat flux over the entire wall:

$$\bar{Q}/\sqrt{(Pe_{2\phi})} = 2\hat{D}(s_w)[s'(0)]. \tag{51}$$

Thus, the average dryout heat flux can be evaluated from

$$\bar{Q}_{dry} = 2.9 \times 10^{-3} Pe_{2\phi}^{1/2} \tag{52}$$

when the fluid properties and porous medium parameters are given and the flow velocity is prescribed. Validation of the dryout prediction, equation (52), is not possible at the present time due to a lack of suitable experimental data, although measurements of the dryout heat flux are available for a volumetrically heated porous bed [19].

7. CONCLUSIONS

A pressure-driven boiling flow adjacent to a heated plate embedded in a capillary porous medium was investigated using the two-phase mixture model developed in Part I. Within the framework of the new formulation, a two-phase boundary layer flow was anticipated. A set of boundary layer equations for the two-phase flow was derived by invoking approximations analogous to the classical boundary layer theory in single-phase fluid dynamics. It was shown that the present problem admits a similarity transformation in which the governing equations are reduced to ordinary differential equations. Illustrative calculations were performed for a water–steam system employing a representative group of constitutive relationships. Results were presented for the saturation profiles, the flow field of the two-phase mixture, the flow fields of the individual phases, as well as for the dependency of the wall heat flux on the wall saturation.

Application of the mixture model to the analysis of a related class of two-phase flow problem, namely purely buoyancy-driven boiling or condensing flows adjacent to a solid surface, is straightforward. These problems also have many important technological applications, and will be the subject of a future publication. In addition, combined pressure- and buoyancy-driven two-phase flows deserve further study in order to test the ability of the present model to predict a counter-current flow pattern.

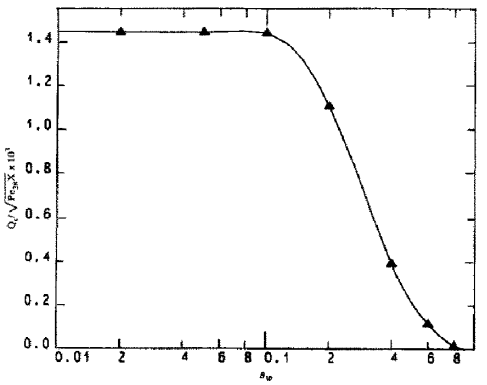

FIG. 8. Dependency of the dimensionless wall heat flux Q_x on the liquid saturation at the wall.

Acknowledgements—This work was supported, in part, by the National Science Foundation under grant No. CTS-8957149.

REFERENCES

1. C.-Y. Wang and C. Beckermann, A two-phase mixture model of liquid–gas flow and heat transfer in capillary porous media—I. Formulation, *Int. J. Heat Mass Transfer* **36**, 2747–2758 (1993).
2. L. M. Cathles, An analysis of the cooling of intrusives by ground-water convection which includes boiling, *Economic Geology* **72**, 804–826 (1977).
3. V. X. Tung and V. K. Dhir, Experimental study of boiling heat transfer from a sphere embedded in a liquid-saturated porous medium, *ASME J. Heat Transfer* **112**, 736–743 (1990).
4. C. Doughty and K. Pruess, A semianalytical solution for heat-pipe effects near high-level nuclear waste packages buried in partially saturated geological media, *Int. J. Heat Mass Transfer* **31**, 79–90 (1988).
5. C. Doughty and K. Pruess, A similarity solution for two-phase fluid and heat flow near high-level waste package emplaced in porous media, *Int. J. Heat Mass Transfer* **33**, 1205–1222 (1990).
6. Y. Ogniewicz and C. L. Tien, Porous heat pipe. In *Heat Transfer, Thermal Control, and Heat Pipes, Progress in Astronautics and Aeronautics* (Edited by W. B. Olstad), Vol. 70, pp. 329–345. AIAA, Washington, D.C. (1979).
7. E. M. Parmentier, Two-phase natural convection adjacent to a vertical heated surface in a permeable medium, *Int. J. Heat Mass Transfer* **22**, 849–855 (1979).
8. P. Cheng and A. K. Verma, The effect of subcooled liquid in film boiling about a vertical heated surface in a porous medium, *Int. J. Heat Mass Transfer* **24**, 1151–1160 (1981).
9. J. Orozco, R. Stellman and M. Gutjahr, Film boiling heat transfer from a sphere and a horizontal cylinder

embedded in a liquid-saturated porous medium, *ASME J. Heat Transfer* **110,** 961–967 (1988).
10. K. S. Udell, Heat transfer in porous media considering phase change and capillarity—the heat pipe effect, *Int. J. Heat Mass Transfer* **28,** 485–495 (1985).
11. O. A. Plumb, D. B. Burnett and A. Shekariz, Film condensation on a vertical plate in a packed bed, *ASME J. Heat Transfer* **112,** 235–239 (1990).
12. A. Majumdar and C. L. Tien, Effects of surface tension on film condensation in a porous medium, *ASME J. Heat Transfer* **112,** 235–239 (1990).
13. J. Orozco, D. Poulikakos and M. Gutjahr, Flow film boiling from a sphere and a horizontal cylinder embedded in a porous medium, *J. Thermophys. Heat Transfer* **2,** 359–364 (1988).
14. C. Y. Wang and C. J. Tu, The effect of non-condensable gas on forced condensation along a horizontal plate in a porous medium, *Int. J. Heat Mass Transfer* **32,** 1847–1852 (1989).
15. I. Fatt and W. A. Klikoff, Effect of fractional wettability on multiphase flow through porous media, *AIME Trans.* **216,** 246–251 (1959).
16. K. S. Udell, Heat transfer in porous media heated from above with evaporation, condensation, and capillary effects, *ASME J. Heat Transfer* **105,** 485–492 (1983).
17. M. C. Leverett, Capillary behavior in porous solids, *AIME Trans.* **142,** 152–169 (1941).
18. IMSL, International Mathematical and Statistical Library (1984).
19. F. P. Tsai, Dryout heat flux in a volumetrically heated porous bed, Ph.D. Dissertation, University of California at Los Angeles (1987).